Experimental and modelled performance of a Ground Penetrating Radar antenna in lossy dielectrics

Craig Warren and Antonios Giannopoulos

***Abstract*—The way in which electromagnetic fields are transmitted and received by Ground Penetrating Radar antennas are crucial to the performance of GPR systems. Simple antennas have been characterised by analysing their radiation patterns and directivity. However there have been limited studies that combine real GPR antennas with realistic environments, which is essential to capture the complex interactions between the antenna and surroundings. We have investigated the radiation characteristics and sensitivity of a GPR antenna in a range of lossy dielectric environments using both physical measurements and a 3D Finite-Difference Time-Domain model. Experimental data was from measured responses of a target positioned at intervals on the circumference of a circle surrounding the H-plane of the antenna. A series of oil-in-water emulsions as well as tap water were used to simulate homogeneous materials with different permittivities and with complex conductivities. Numerical radiation patterns were created utilising a detailed 3D FDTD model of the antenna. Good correlation was shown between the experimental results and modelled data with respect to the strength of the main lobe within the critical angle window. However, there are discrepancies in the strength of main lobe at shallow angles. In all the dielectrics the main lobes are generally broad due to the near-field observation distance but, as expected, become narrower with increasing permittivity. These results provide confidence for further use of the FDTD antenna model to investigate scenarios such as larger observation distances and heterogeneous environments that are difficult to study experimentally.**

***Index Terms*—Antenna measurements, antenna radiation patterns, broadband antennas, electromagnetic modelling, Finite-Difference Time-Domain (FDTD)**

I. Introduction

Ground Penetrating Radar (GPR) is used in a wide range of different applications in the fields of engineering and geophysics. The diversity of GPR usage has meant there are a number of different GPR antenna designs used in industry and also within the academic community for research. The type and size of a GPR antenna is usually dependent on the application, e.g., low frequency antennas, which are physically larger, are used where significant depth of penetration is important, whereas high frequency antennas, which are physically smaller, are used where less penetration and better resolution are required. Understanding how energy is transmitted and received by a particular GPR antenna has many benefits: improved antenna design, enhanced data processing and inversion algorithms, better informed usage of the antenna in GPR surveys, and improved interpretation of GPR responses. The radiation characteristics of antennas are usually investigated by studying the radiation patterns and directivity. For GPR antennas it is also important to study these characteristics when the antenna is in different environments that would typically be encountered in GPR surveys. This is because interactions between the antenna and the environment change how the antenna behaves.

Studies of antenna radiation characteristics can, largely, be divided into three areas: theoretical analysis, experimental/measured data, and numerical modelling. The theoretical radiation patterns of simple antennas, such as the cylindrical monopole, can be completely predicted in free-space [1]. Another example is the infinitesimal dipole which in free-space exhibits two-dimensional (2D) patterns that are sections of the classic torus shape. There are also theoretical approximations for the far-field patterns of infinitesimal dipole antennas over lossless [2] and low-loss [3] half-spaces.

The radiation pattern of one antenna can be measured directly with a second antenna, and this has been done in free-space for simple antennas as well as for more widely-used commercial GPR antennas [4]–[6]. There are also laboratory measurements of radiation patterns of simple antennas over homogeneous materials obtained directly with another antenna [7], and indirectly through the recording of responses from a simple target [6], [8]. Measuring antenna radiation patterns in free-space requires an antenna range with accurate positioning equipment, and the outcome is of limited use for GPR. Directly measuring antenna radiation patterns in realistic materials, which is useful for GPR, presents many practical difficulties. This has prompted numerical simulations of GPR antenna radiation patterns. A comparison of theoretical, measured, and modelled radiation patterns of infinitesimal dipoles located over lossless and low-loss half-spaces is provided by [9].

The state of numerically derived GPR antenna radiation patterns is similar to that of measured data, i.e., simple and more complex antennas have been modelled in free-space, simple antennas have been modelled in realistic environments, but there have been very limited studies that combine real GPR antenna models with realistic environments. Reference [10] modelled an off-ground stepped-frequency continuous-wave (SFCW) horn antenna over layered media using linear transfer functions. Near-field [11] antenna models using equivalent sets of infinitesimal electric dipoles have also been developed for use over layered media. The energy distribution of a shielded dipole antenna over various lossless half-spaces has been studied by [12].

This paper presents an investigation of the radiation characteristics and sensitivity of a commercially-available high-

frequency GPR antenna, using experimental and modelled data. The complex interactions of the antenna (with all its loading, shielding, absorbers etc...) over a range of different and lossy dielectrics are studied. Firstly, the apparatus and experimental procedure that was used to measure data from the 1.5 GHz commercial GPR antenna is described. Emulsions were used to simulate materials with different permittivities and conductivities. Next, the Finite-Difference Time-Domain (FDTD) antenna model that was developed and used to create numerical radiation patterns is described. The antenna model replicates all the detailed geometry and main components of the real antenna. Finally, the paper focuses on comparing the measured and modelled patterns, and using them to analyse the radiation characteristics of the antenna.

II. Experimental apparatus and methodology

A series of experiments were conducted to characterise the radiation dynamics and sensitivity of a commonly used high-frequency GPR antenna — a Geophysical Survey Systems, Inc. (GSSI) 1.5 GHz antenna — in different dielectric environments. This type of GPR antenna is primarily used for the evaluation of structural features in concrete. A series of oil-in-water (O/W) emulsions were used to simulate materials with different dielectric properties. The permittivity and conductivity of the emulsions were set by controlling ratios of the constituent chemicals [13]. A further advantage of using liquids was the ease with which targets could be positioned and repositioned. Three emulsions were used with relative permittivities of 5, 10, and 30, and complex conductivities. Tap water with relative permittivity 72 was also used, which provided a total of 4 different lossy dielectric test environments. The electrical properties of the emulsions can be derived using the Hanai-Bruggeman (HB) formula. It has been shown that for frequencies less than 4 GHz the relative permittivity of an emulsion is approximately constant. However, the conductivity is given by a constant DC term plus a term that increases with the square of frequency [14]. To replicate this behaviour in the simulation a Debye model with an additional constant DC conductivity term was used. The parameters of the Debye model were adjusted to fit the complex conductivity from the HB formula. Fig. 1a shows the relative permittivities of the emulsions and tap water used in the model (the real part of the Debye equation) over a frequency bandwidth of interest for the antenna. Fig. 1b shows the complex conductivities of the emulsions and tap water from both the HB formula and the Debye-based model (imaginary part of the Debye equation plus a constant conductivity term) over a frequency bandwidth of interest for the antenna.

The main components of the experimental apparatus were: a 50 litre galvanised steel tank (610 mm $\times$ 400 mm $\times$ 210 mm); a plastic rig to mount and position the antenna and target; and a high-shear batch mixer and plastic mixing vessel; and the GPR system and antenna. A 12 mm steel rebar was used as a target to measure the back-scattered response from, and hence investigate the radiation characteristics of the antenna. A rebar was chosen as it is a typical target for such a high-frequency GPR antenna. The rebar could be positioned at 6° increments

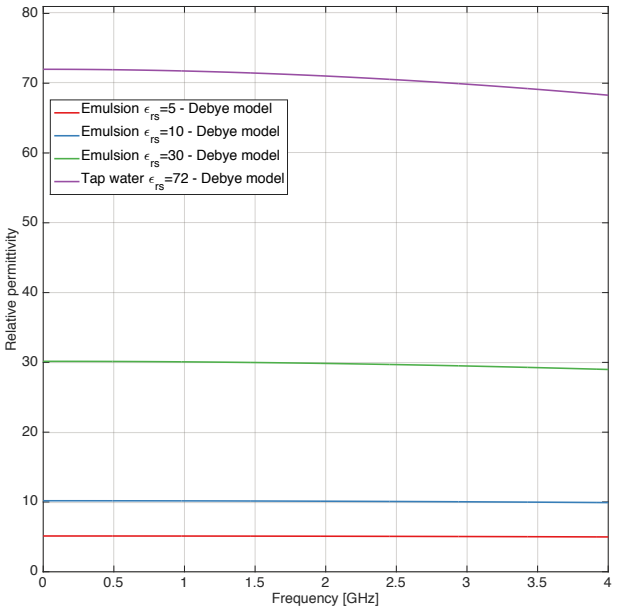

(a) Relative permittivities

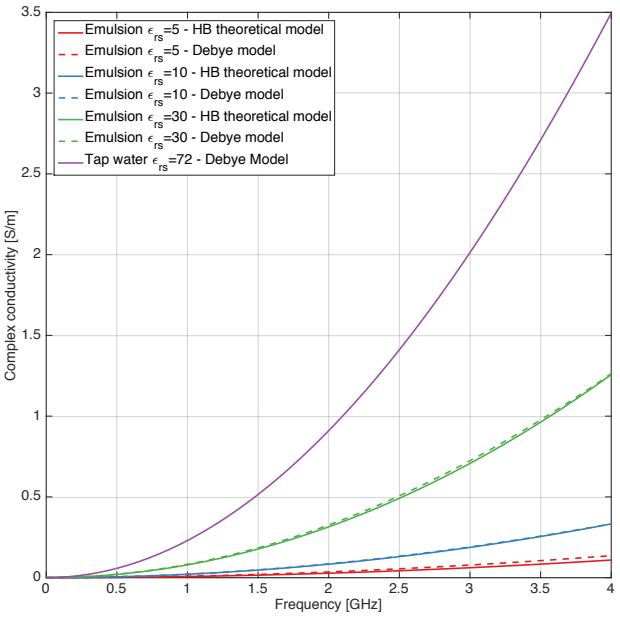

(b) Complex conductivities - theoretical Hanai-Bruggeman (HB) model based on the emulsion chemistry; Debye-based model used in the simulations

Fig. 1. Relative permittivities and complex conductivities of the emulsions and tap water

on a circle of radius 110 mm around the antenna (centre taken as the mid-point between the transmitting (T_x) and receiving (R_x) elements of the antenna). It was not possible to conduct tests at larger radii due to the excessive volumes of liquid required.

The first step of the experimental procedure was to mix the emulsion until it became a visually homogeneous medium. Prior work [13] had shown that mixing the emulsion continually for a period of 15 minutes using the high-shear batch mixture would ensure it would be stable for several days (and therefore more than sufficient for the 1-2 hours duration of each experiment). The permittivity of the emulsion was then checked by recording responses from an empty tank with the tank base adjusted to two different height positions. Knowledge of the internal antenna geometry and the tank dimensions meant a theoretical path distance could be calculated. Combined with the time difference between the two responses recorded by the GPR system, a velocity and hence permittivity for each emulsion was calculated. This was checked against the designed permittivity value for each emulsion and rechecked at the end of each series of measurements to ensure it remained stable. This indirect measurement method incurred an error of $\pm 3\%$ in permittivity values but was used as there was no equipment available to measure permittivity directly.

Measurements to characterise the radiation dynamics and sensitivity of the antenna began by placing the antenna on the surface of the liquid and recording a response from the tank with no target (rebar) present. This reading was used for background removal in subsequent measurements that included the target. The rebar was then inserted into each of the holes in the plastic rig in turn. At each position the response was recorded for approximately 10 seconds duration from which an average response was obtained. This experimental procedure was repeated for the three emulsions and water.

III. Finite-Difference Time-Domain numerical model

All of the simulations conducted for this research used gprMax3D which is part of gprMax, a suite of electromagnetic wave simulators based on the FDTD method. gprMax (http://www.gprmax.com/) is freely available software that was written by [15] originally in 1996, and has since developed into a mature application that has been successfully used by a number of researchers [16]–[19]. The simulations included a model of the antenna that is representative of the GSSI 1.5 GHz antenna used in the experimental tests. The antenna model includes all of the main features and geometry of the real antenna. Details of the antenna model development and the subsequent initial validation can be found in [13].

Planar bowties are used for the T_x and R_x elements of the antenna. The bowties have a flare angle of 76° and additional rectangular patches added to their open ends. These extensions perform like straight sections of waveguide, which introduce a delay in the signal path and create destructive interference patterns that reduce unwanted resonance. The bowties are etched from copper onto the Printed Circuit Boards (PCB), and

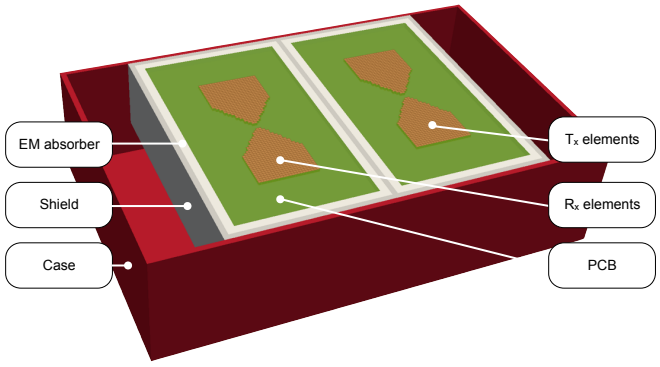

Fig. 2. FDTD mesh of antenna model (main features annotated)

enclosed in rectangular metal boxes which shield the antenna. An open-cell carbon-loaded foam acts as an ultra-wideband (UWB) electromagnetic absorber to reduce unwanted resonance and is used in the cavities behind the bowties. Generally, carbon-loaded UWB microwave absorbers, e.g., Emerson and Cuming ECCOSORB LS (http://www.eccosorb.com), have a permeability of 1 but can have permittivities ranging from 1.25 to 30.

The excitation of the antenna — pulse shape, frequency content, and feed method — is important for the performance of the real antenna, and hence critical to capture in the model. In common with many other GPR simulations [20]–[23] a Gaussian shaped pulse was assumed with a centre frequency of 1.5 GHz. A simple Gaussian shape is a good approximation, but may not be an entirely realistic representation of the real pulse which is often generated by an avalanche transistor. A feed model consisting of a voltage source with internal resistance inserted in a one-cell gap between the two arms of the transmitter bowtie (the drive-point) was used.

Fig. 2 shows the detailed FDTD mesh of the geometry of the antenna, and Fig. 3 shows the FDTD mesh of the experimental apparatus. A spatial discretisation of $\Delta x = \Delta y = \Delta z =$ 1 mm was chosen as a good compromise between accuracy and computational requirements. GprMax computes the spatial and temporal derivatives using a standard second-order scheme and this choice of spatial discretisation also ensured that any numerical dispersion was adequately controlled. The Courant Friedrichs Lewy (CFL) condition was enforced which resulted in a time-step of Δt = 1.926 ps.

The three emulsions (and the tap water) used in the experiments have frequency-dependent conductivities [13] which were modelled by fitting a Debye formulation [24].

IV. Experimental and numerical antenna radiation patterns

Traditionally antenna patterns are plotted at a specific single frequency, however this is of limited use in analysing the overall performance of an UWB GPR antenna. For both the experimental and modelled data, measures of the received energy were taken using Eq. (1) proposed by [12].

$$E_{tot}(r,\theta) = \sum_{t}^{T} \frac{E(r,\theta)^2}{Z} \tag{1}$$

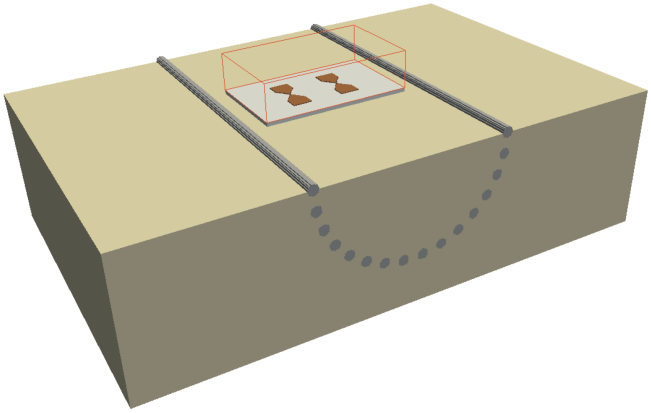

Fig. 3. FDTD model of the experimental apparatus (only a selection of rebar positions are shown; the tank and some details of the antenna are omitted for illustrative purposes). N.B. Measurements were made with a single rebar at each of locations in turn.

E_{tot} is the total energy at a specific radius (r) and angle (θ); the summation is made over a time-domain response; E is the electric field value at a given radius (r) and angle (θ); and Z is the electromagnetic impedance of the medium.

In the laboratory experiments, at each rebar position, a background response (with no rebar present) was subtracted from an A-scan with the rebar. A time-gate was used to isolate the reflected wavelet from the rebar. Eq. (1) was then applied to produce a measure of the energy in the reflected wavelet from the rebar at that radius and angular position. It was found that Eq. (1) produced similar results to a metric that picked the maximum positive peak of the reflected wavelet from the rebar. Data from the laboratory experiments was collected with the antenna in a single orientation. This allowed only the H-plane pattern to subsequently be studied, however it is of most interest for GPR as it is usually parallel to the survey direction. The back lobe, i.e., the part in air, of the pattern has been omitted from the plots. This is because a measure of the energy from the rebar wavelet in air was difficult to reliably obtain from the experimental data.

All patterns are plotted on a logarithmic scale unless otherwise stated. A solid grey line represents the boundary between air and the dielectric environment. Solid grey lines are also used to indicate the critical angle window.

Table I presents electromagnetic wave properties for the dielectric environments that were used in the experiments. The

TABLE I
PROPERTIES OF THE DIELECTRIC ENVIRONMENTS ($f_c = 1.5$ GHz)

ϵ_r	θ_c (°)	λ (m)	R (m)	r/λ
5	27	0.089	0.081	1.23
10	18	0.063	0.114	1.74
30	11	0.037	0.197	3.02
72	7	0.024	0.306	4.67

critical angle in the dielectric environment is given by θ_c, and r is the principle observation distance (0.11 m). Wavelengths and critical angles are properties associated with a specific single frequency (in this case $f_c = 1.5$ GHz), so are of limited use in analysing the overall performance of an UWB GPR antenna. However, they are still commonly used and hence are given here. The observation distance was limited by the physical constraints of the apparatus, and the need to be able to clearly identify the wavelet reflected from the rebar in all responses. Despite this, target detection at a distance of 0.11 m is still a valid application of such a high-frequency antenna. The r/λ ratio is the observation distance in wavelengths. R is theoretical boundary between the radiating near-field and far-field of the antenna [25], calculated using Eq. (2). R is also rather an ill-defined property to use when analysing an UWB antenna.

$$R = \frac{2D^2}{\lambda} \tag{2}$$

D is the largest dimension of the antenna (0.060 m), and λ is the wavelength in the medium.

Fig. 4 presents the H-plane patterns from the experimental data in the different dielectric environments. As expected all of the patterns show a broad main lobe with maximum power directly under the antenna (180°). As the permittivity of the dielectric environment increases the main lobe becomes narrower, e.g., in the tap water ($\epsilon_r = 72$) it is approximately 6 dB narrower than the lowest permittivity emulsion ($\epsilon_r = 5$) at angles beyond 150°,210°. This occurs because as the critical angle becomes smaller as the permittivity of the dielectric environment increases. Energy in the critical angle window mainly comes from the spherical ground wave, whereas energy beyond the critical angle window is associated with lateral waves. It can be observed that, despite T_x and R_x elements of the antenna being offset from each another, the H-plane pattern is symmetric about the vertical axis (0°,180°). This is because the path distance (from T_x to the rebar target to R_x) is the same for radial positions on either side of the vertical axis.

As a verification of the experimental methodology and data processing, measurements were also made at an observation distance of $r = 0.15\ m$. Figs. 5, 6 & 7 show comparisons of the H-plane patterns from the experimental data at the two different observation distances[1]. There are some small differences at shallow angles in the dielectric of permittivity 10, but overall the patterns at the two radii in the different dielectrics are well matched. This gives confidence in the experimental approach and also shows there is little change in the antenna behaviour at these observation distances.

Fig. 8 is included to show the traditional single frequency method of plotting an antenna pattern. The frequency used is the centre frequency of the antenna ($f_c = 1.5$ GHz), which corresponds to an observation distance 3 wavelengths in the emulsion of permittivity $\epsilon_r = 5$. As stated previously, patterns plotted at a specific single frequency are of limited use in analysing the overall performance of an UWB GPR antenna.

Figs. 9 to 12 present comparisons of the H-plane patterns from experimental data with the FDTD numerical model in the different dielectric environments. In Fig. 9 the observation distance of 0.11 m (1.23 λ) from the antenna is theoretically in

[1]A comparison in the dielectric of permittivity 5 is not given because it was impossible to clearly separate the rebar wavelet from the reflection of the bottom of the tank at an observation distance of $r = 0.15\ m$.

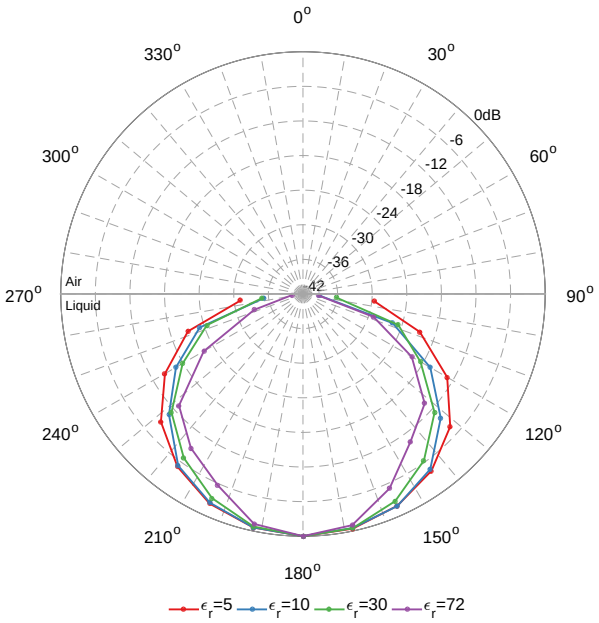

Fig. 4. Experimental 'received energy' H-plane patterns observed at $r = 0.11\ m$.

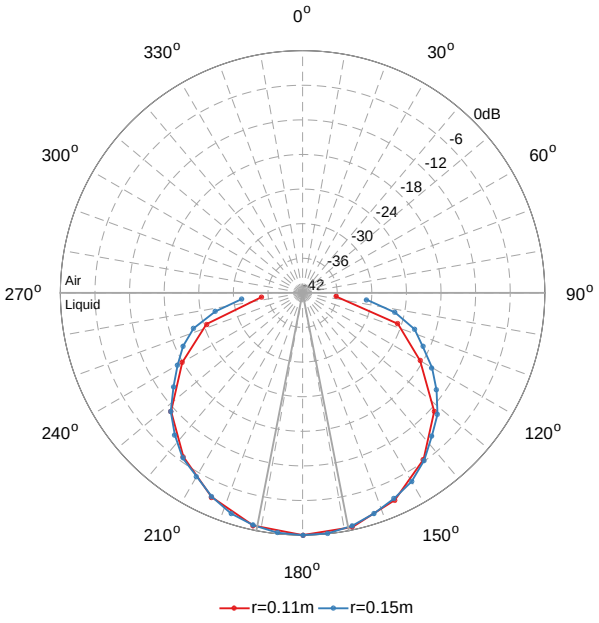

Fig. 6. Experimental 'received energy' H-plane patterns in emulsion of permittivity $\epsilon_r = 30$ at radii $r = 0.11\ m$ and $r = 0.15\ m$.

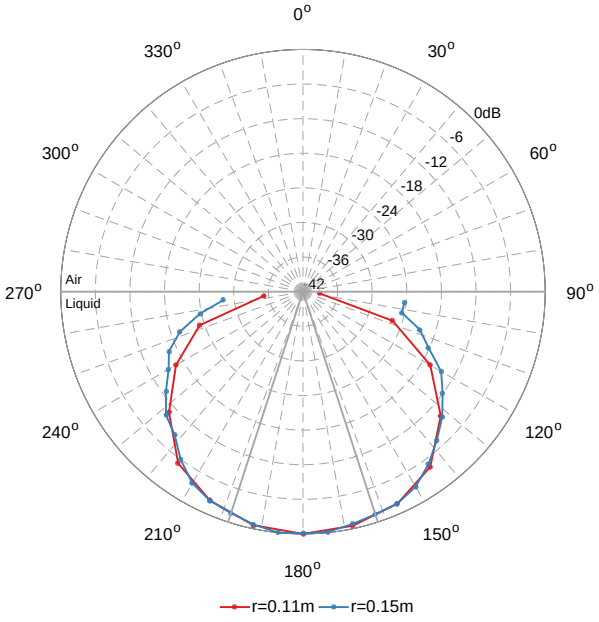

Fig. 5. Experimental 'received energy' H-plane patterns in emulsion of permittivity $\epsilon_r = 10$ at radii $r = 0.11\ m$ and $r = 0.15\ m$.

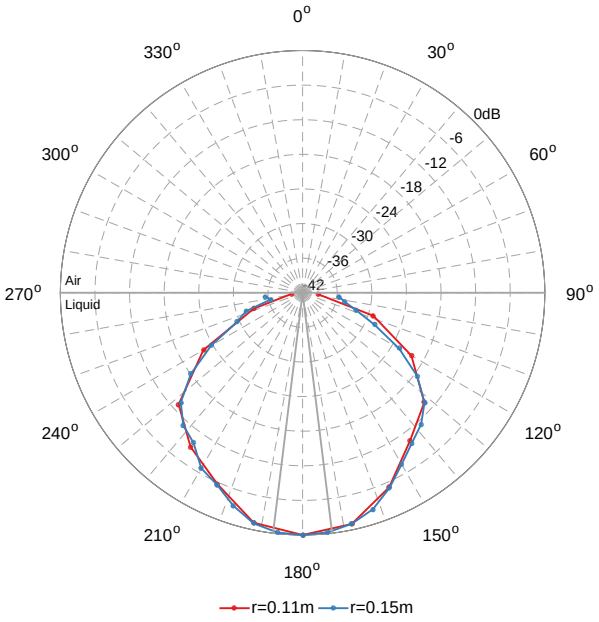

Fig. 7. Experimental 'received energy' H-plane patterns in emulsion of permittivity $\epsilon_r = 72$ at radii $r = 0.11\ m$ and $r = 0.15\ m$.

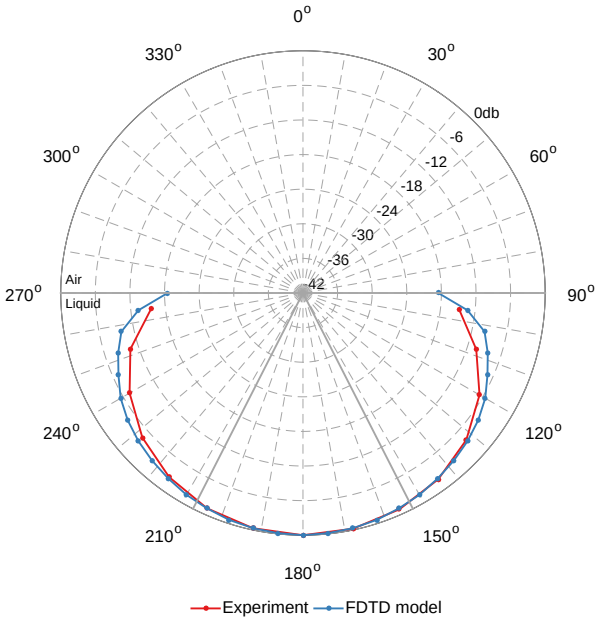

Fig. 8. Experimental and modelled 'received energy' H-plane patterns in emulsion of permittivity $\epsilon_r = 5$ at radius $r = 0.11\ m$. N.B. For this figure only, using the traditional single frequency method, where $f = f_c = 1.5$ GHz.

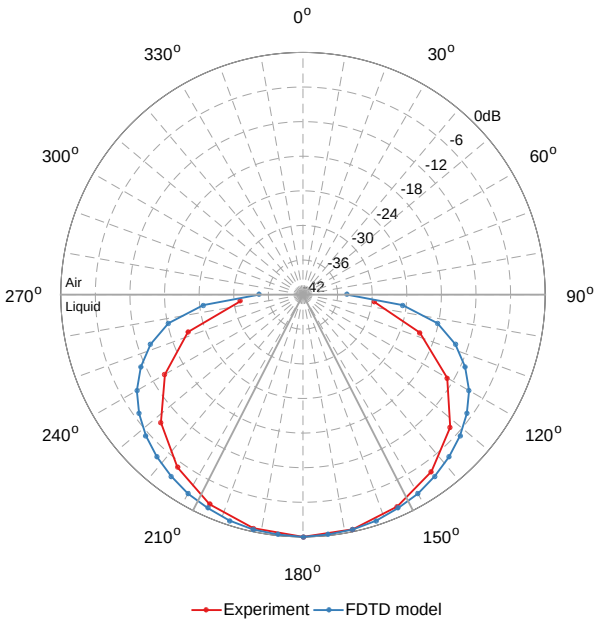

Fig. 9. Experimental and modelled 'received energy' H-plane patterns in emulsion of permittivity $\epsilon_r = 5$ at radius $r = 0.11\ m$.

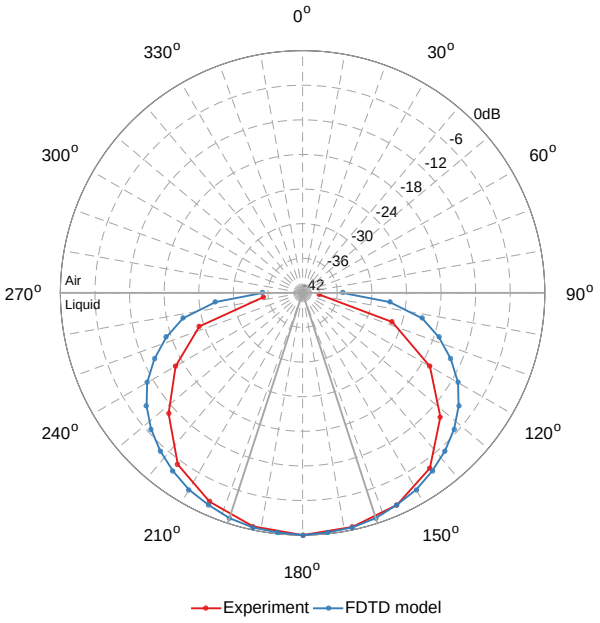

Fig. 10. Experimental and modelled 'received energy' H-plane patterns in emulsion of permittivity $\epsilon_r = 10$ at radius $r = 0.11\ m$.

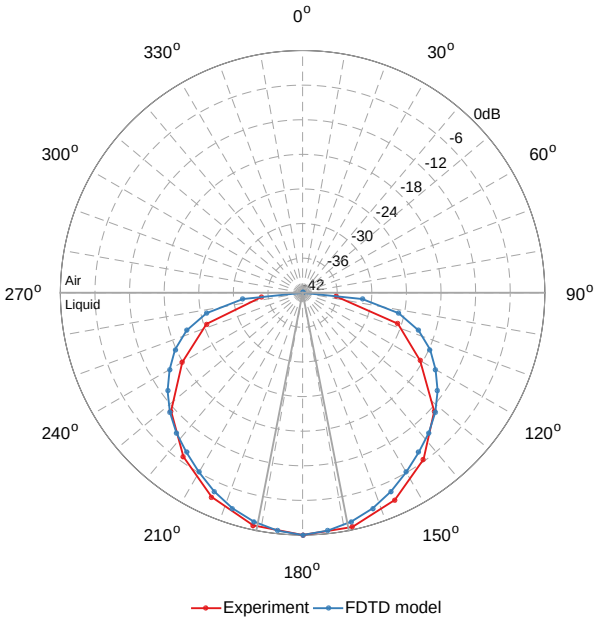

Fig. 11. Experimental and modelled 'received energy' H-plane patterns in emulsion of permittivity $\epsilon_r = 30$ at radius $r = 0.11\ m$.

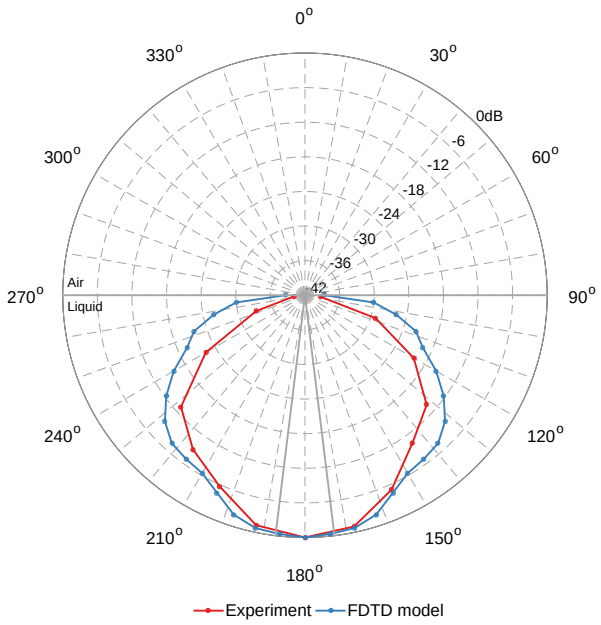

Fig. 12. Experimental and modelled 'received energy' H-plane patterns in water of permittivity $\epsilon_r = 72$ at radius $r = 0.11\ m$.

the far-field ($R = 0.081\ m$). However, this boundary definition is fuzzy when applied to an impulse-driven UWB antenna, in fact studies [9] and [12] have suggested far-field behaviour does not begin to become apparent until a distance of 10λ from the antenna. In Fig. 9 both experimental and modelled patterns show a broad main lobe with maximum power directly under the antenna (180°), decreasing to half-power (-3 dB) just beyond the critical angle (153°, 207°). The FDTD model begins to over-predict the power of the experimental pattern beyond the critical angle, with a maximum discrepancy of 6 dB at around 120° and 240°.

In Fig. 10 the behaviour is similar except that half-power now occurs beyond, rather that at, the critical angle (162°, 198°) at 145° and 215°. In Fig. 11 the correlation between the experimental and modelled results is improved but there are still differences of 3 dB at shallow angles. Fig. 12 presents the results from tap water. The main lobe has narrowed and side lobes are beginning to appear in both experimental and modelled patterns at around 135° and 225°. It is also around these angles the modelled pattern deviates from the measured pattern, over-predicting by up to 6 dB. The differences between the modelled and measured patterns beyond the critical angle window are systematic, i.e., they are a similar feature in all the dielectric environments. This suggests they cannot be attributed to problems in accurately modelling the emulsion properties. The most likely explanation is that the FDTD antenna model does not capture the way in which lateral waves propagate from the real antenna. The FDTD antenna model is a very good representation of the real antenna (including all of the main features and geometry) but because of commercial sensitivity cannot include every detail. Even if this were possible, intrinsically there will always be small differences between a model and reality.

V. Conclusion

The investigation of radiation characteristics of an antenna makes it possible to develop a better understanding of how the antenna radiates and receives energy. This is important for GPR as, for example, it can lead to a better understanding of the spatial resolution of a GPR antenna and how it can discriminate between closely spaced targets.

Physical measurements of the sensitivity of a high-frequency GPR antenna have been made in lossy dielectrics with a range of different permittivities. These measurements were made in the near-field of the antenna at a observation distance that shallow targets may typically be detected. For the range of permittivities studied, the H-plane patterns exhibit broad main lobes, but without the nulls present at the critical angles in analytical far-field patterns. Comparison between these measured patterns and those generated from a 3D FDTD model is generally good, but differences exist particularly at shallow angles outwith the critical angle window.

The results from this series of experiments serve to validate the numerical antenna model for use in more extensive studies. This is particularly useful for studies at a range of observation distances and in other dielectric environments that are difficult to investigate experimentally.

Acknowledgment

This work has made use of the resources provided by the Edinburgh Compute and Data Facility (ECDF) (http://www.ecdf.ed.ac.uk/)

This work benefited from networking activities carried out within the EU funded COST Action TU1208 "Civil Engineering Applications of Ground Penetrating Radar."

References

[1] R. W. King, *Theory of Linear Antennas with Charts and Tables for Practical Applications*. Harvard University Press, 1956.

[2] N. Engheta, C. Papas, and C. Elachi, "Radiation patterns of interfacial dipole antennas," *Radio Science*, vol. 17, pp. 1557–1566, 1982.

[3] G. Smith, "Directive properties of antennas for transmission into a material half-space," *IEEE Transactions on Antennas and Propagation*, vol. 32, no. 3, pp. 232–246, 1984.

[4] S. Millard, A. Shaari, and J. Bungey, "Field pattern characteristics of GPR antennas," *NDT and E International*, vol. 35, no. 7, pp. 473–482, 2002.

[5] G. Klysz, X. Ferrieres, J. Balayssac, and S. Laurens, "Simulation of direct wave propagation by numerical FDTD for a GPR coupled antenna," *NDT and E International*, vol. 39, no. 4, pp. 338–347, 2006.

[6] V. Pérez-Gracia, D. Di Capua, R. González-Drigo, and L. Pujades, "Laboratory characterization of a GPR antenna for high-resolution testing: Radiation pattern and vertical resolution," *NDT and E International*, vol. 42, no. 4, pp. 336–344, 2009.

[7] A. Annan, W. Waller, D. Strangway, J. Rossiter, J. Redman, and R. Watts, "The electromagnetic response of a low-loss, 2-layer, dielectric earth for horizontal electric dipole excitation," *Geophysics*, vol. 40, pp. 285–298, 1975.

[8] S. Arcone, "Numerical studies of the radiation patterns of resistively loaded dipoles," *Journal of Applied Geophysics*, vol. 33, pp. 39–52, 1995.

[9] S. Radzevicius, C. Chen, L. Peters, and J. Daniels, "Near-field dipole radiation dynamics through FDTD modeling," *Journal of Applied Geophysics*, vol. 52, no. 2-3, pp. 75–91, 2003.

[10] S. Lambot, E. C. Slob, I. van den Bosch, B. Stockbroeckx, and M. Vanclooster, "Modeling of ground-penetrating radar for accurate characterization of subsurface electric properties," *Geoscience and Remote Sensing, IEEE Transactions on*, vol. 42, no. 11, pp. 2555–2568, 2004.
[11] S. Lambot, F. André, E. Slob, and H. Vereecken, "Effect of antenna-medium coupling in the analysis of ground-penetrating radar data," *Near Surface Geophysics*, vol. 10, no. 6, pp. 631–639, 2012.
[12] N. Diamanti and A. P. Annan, "Characterizing the energy distribution around gpr antennas," *Journal of Applied Geophysics*, vol. 99, pp. 83–90, 2013.
[13] C. Warren and A. Giannopoulos, "Creating FDTD models of commercial GPR antennas using Taguchi's optimisation method," *Geophysics*, vol. 76, no. 37, 2011.
[14] G. Smith and W. Scott, "The use of emulsions to represent dielectric materials in electromagnetic scale models," *IEEE Transactions on Antennas and Propagation*, vol. 38, no. 3, pp. 323–334, 1990.
[15] A. Giannopoulos, *GprMax - FDTD based GPR simulation software*, 2005.
[16] L. Galagedara, J. Redman, G. Parkin, A. Annan, and A. Endres, "Numerical modeling of GPR to determine the direct ground wave sampling depth," *Vadose Zone Journal*, vol. 4, pp. 1096–1106, 2005.
[17] M. Jeannin, S. Garambois, C. Grégoire, and D. Jongmans, "Multiconfiguration GPR measurements for geometric fracture characterization in limestone cliffs (Alps)," *Geophysics*, vol. 71, p. B85, 2006.
[18] O. Lopera and N. Milisavljevic, "Prediction of the effects of soil and target properties on the antipersonnel landmine detection performance of ground-penetrating radar: A Colombian case study," *Journal of Applied Geophysics*, vol. 63, no. 1, pp. 13–23, 2007.
[19] F. Soldovieri, J. Hugenschmidt, R. Persico, and G. Leone, "A linear inverse scattering algorithm for realistic GPR applications," *Near Surface Geophysics*, vol. 5, no. 1, pp. 29–42, 2007.
[20] L. Gurel and U. Oguz, "Three-dimensional FDTD modeling of a ground-penetrating radar," *IEEE Transactions on Geoscience and Remote Sensing*, vol. 38, no. 4, pp. 1513–1521, 2000.
[21] K.-H. Lee, C.-C. Chen, F. Teixeira, and R. Lee, "Modeling and investigation of a geometrically complex UWB GPR antenna using FDTD," *IEEE Transactions on Antennas and Propagation*, vol. 52, no. 8, pp. 1983–1991, 2004.
[22] Y. Nishioka, O. Maeshima, T. Uno, and S. Adachi, "FDTD analysis of resistor-loaded bow-tie antennas covered with ferrite-coated conducting cavity for subsurface radar," *IEEE Transactions on Antennas and Propagation*, vol. 47, no. 6, pp. 970–977, 1999.
[23] R. L. Roberts and J. J. Daniels, "Modeling near-field GPR in three dimensions using the FDTD method," *Geophysics*, vol. 62, no. 4, pp. 1114–1126, 1997.
[24] P. Debye, "Polare Molekeln," *Leipzig: Hirzel,— c1929*, 1929.
[25] J. Kraus, *Electromagnetics*. WCB/McGraw-Hill, 1991.

Craig Warren received the degrees of B.Eng. in Electrical and Mechanical Engineering, and Ph.D. in Engineering from The University of Edinburgh, U.K. in 2003 and 2009, respectively. From 2010 to 2013 he held the positions of Teaching Fellow and Learning Technologist, and is currently a Research Associate at The University of Edinburgh, U.K. His main research interests are the development of numerical models of Ground Penetrating Radar, and novel applications of GPR to engineering problems. He is also active in the field of engineering education and technology enhanced learning. He is a Chartered Engineer (C.Eng.), Fellow of The Higher Education Academy (FHEA), U.K., and a member of both the Institution of Mechanical Engineers (IMechE), U.K, and the Institution of Engineering Technology (IET), U.K.

Antonios Giannopoulos received a B.Sc. (1991) in Geology from the Aristotle University of Thessaloniki, Greece and a D.Phil. (1997) in Electronics from The University of York, UK. Since 2009, he is a Senior Lecturer in the School of Engineering, Institute for Infrastructure and Environment, at The University of Edinburgh, UK. His research interests include the numerical modelling of ground penetrating radar and the development and application of geophysical techniques for non-destructive testing and condition assessment of structures and transport systems. He is the author of GprMax (www.gprmax.com) a freely available FDTD GPR simulator. He is a member of SEG and EAGE.